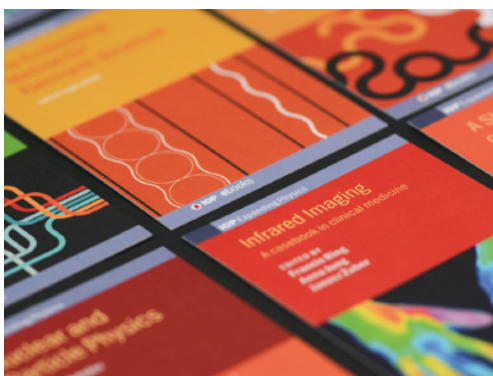


PAPER

Transverse-pressure susceptibility of high- J_c RRP and PIT types of Nb_3Sn Rutherford cables for accelerator magnets

To cite this article: P Gao *et al* 2020 *Supercond. Sci. Technol.* **33** 125005

View the [article online](#) for updates and enhancements.




IOP | ebooks™

Bringing together innovative digital publishing with leading authors from the global scientific community.

Start exploring the collection—download the first chapter of every title for free.

Transverse-pressure susceptibility of high- J_c RRP and PIT types of Nb_3Sn Rutherford cables for accelerator magnets

P Gao^{1,2} , M Dhallé², B Bordini³, A Ballarino³ and H H J Ten Kate²

¹ The Institute of Plasma Physics, CAS, Hefei 230031, People's Republic of China

² University of Twente, P.O. Box 217, 7500 AE Enschede, The Netherlands

³ CERN, European Organization for Nuclear research, 1211 Geneva 23, Switzerland

E-mail: phdgaop@gmail.com

Received 19 July 2020, revised 23 August 2020

Accepted for publication 16 September 2020

Published 26 October 2020



CrossMark

Abstract

In the frame of the High-Luminosity Large Hadron Collider construction and Future Circular Collider development program, the magnetic field in the accelerator dipole magnets is being enhanced to 11 T, and 15 T to 16 T level, respectively. Advanced Nb_3Sn superconductors with a non-copper critical current density exceeding 2500 A mm^{-2} at 4.2 K and 12 T, are being developed using the Restacked-Rod-Process (RRP) and Powder-In-Tube (PIT) wire technologies. However, since Nb_3Sn is extremely brittle, it is a significant challenge to construct the high-field dipole magnets with such very strain-susceptible superconductor. The high-level of stress acting on the wide face of the Rutherford cables in the coils of 120 MPa to 200 MPa generated by the Lorenz' force, causes initially a reversible reduction and eventually at some stress level followed by permanent degradation of the critical current when strain goes to high. This study sets out to examine the critical current and upper critical field performance of state-of-the-art RRP and PIT Nb_3Sn Rutherford cables in terms of transverse pressure. The variation of the critical current and upper critical field due to the thermal- and mechanical load-cycling was investigated as well. For reference, the critical current of witness wires characterized on standard ITER type barrels were also measured. The results indicate that the RRP type of Nb_3Sn Rutherford cables, when fully impregnated with epoxy resin, are able to withstand a transverse stress of 170 MPa to 250 MPa without noticeable irreversible critical current reduction. For the transverse pressure limit for present PIT type of Nb_3Sn Rutherford cables somewhat lower values are found at the level of 50 MPa to 120 MPa. Therefore, given the present cables, the high-field dipole magnet construction can be realized using the RRP Nb_3Sn Rutherford cables, while for PIT type cables more cable development is requested to enhance the onset of irreversible degradation. The reversible critical current reduction in RRP type of cables of 10% at 150 MPa to 250 MPa needs to be taken into account when predicting magnet performance. Finally, extreme care needs to be taken into account for Nb_3Sn coil fabrication, since the experimental results show significant critical current

reduction due to stress concentrations already at 0.2° misalignment angles between the pressure applying surface and the surface of the impregnated cable.

Keywords: RRP and PIT Nb₃Sn wire, Rutherford cable, transverse pressure, critical current degradation

(Some figures may appear in colour only in the online journal)

1. Introduction

For the High-Luminosity Large Hadron Collider (HL-LHC) Nb₃Sn dipole and quadrupole magnets are required and their construction is underway [1]. In parallel, more advanced Nb₃Sn magnet technology is being developed for the 15 T to 16 T class dipole magnets requested for the Future Circular Collider providing proton-proton collisions at 100 TeV level, through the so-called Short Model Coil (SMC) development program at CERN [2] and supporting the construction of a few 15 T to 16 T short model dipole magnets [3]. For this purpose, advanced Nb₃Sn conductors, with a non-copper critical current density exceeding 2500 A mm^{-2} at 4.2 K and 12 T, are being developed using the ‘Restacked-Rod-Process’ (RRP) [4] and the ‘Powder-In-Tube’ (PIT) process [5], provided by Bruker-OST in the USA and Bruker-EAS in Europe, respectively.

Nb₃Sn intrinsically is a brittle material, and the construction of high-field dipole and quadrupole magnets with such strain-susceptible superconductor is a significant challenge taking many years of development. The cause of strain-induced critical current reduction in Nb₃Sn conductors during dipole magnet fabrication can be addressed as follows: (1) mechanical stress applied to strands and cables during cabling, coil winding and magnet assembly process; (2) thermal strain generated during conductor-in-coil heat-treatments and cool-down to operational temperatures; (3) Lorentz force acting on the wide surface of the impregnated coil turns when energizing the magnets. The deformation of wires with Nb and Sn sources (unreacted Nb₃Sn) during cabling needs to be controlled in order to balance the reduction of the critical current against the gain in engineering critical current density of Rutherford cables [6, 7]. The pre-stress applied on the cables in heat-treated coils has to be kept below the irreversible transverse stress limit, taking into account the thermal stress generated during magnet cool-down. For high-field accelerator magnets, ensuring that the superconducting Nb₃Sn in the coils is capable to sustain the high-level stress caused by the Lorentz force remains the most significant challenge.

The predicted level of transverse stress acting on the wide face of the Rutherford cables are in the range of 100 MPa to 150 MPa for the 11 T cosine-theta coil configuration [1] and 150 MPa to 200 MPa for 16 T dipole magnets flavored in various coil configurations types following cosine-theta [8], block [9], common-coil [10], and canted-cosine-theta [11]. Generally, transverse stress exerted on the cable surface initially causes a reversible reduction of the critical current associated with Nb₃Sn lattice deflection, while at some higher stress a permanent, thus irreversible degradation of the critical current

sets in essentially due to cracking of the Nb₃Sn filaments in the wire.

Historically, the first multi-filamentary Nb₃Sn wires were mainly produced using the so-called ‘bronze-process’ in the 1970s [12], and early studies on transverse pressure susceptibility of Nb₃Sn Rutherford cables were based on this type of superconducting wires. A bronze-process Nb₃Sn Rutherford cable reported by Jakob *et al* [13] started to degrade significantly beyond 70 MPa and the critical current reached 60% at 150 MPa at 4.2 K and 12 T. Moreover, it was observed that the critical current of similar cable samples with solder-filling exhibited less degradation at 150 MPa, but still at -30% level. The reason for this behavior was hinted to be the relatively soft solder matrix distributing the load among the strands. This can result in a lower local pressure on the strands in the solder-filled cable compared to a bare cable. Further research on the same type of key-stoned Rutherford cables by Jakob *et al* [14] indicated that with epoxy resin impregnation, the critical current reduction of cables may be reduced by 5% at 150 MPa.

For a key-stoned cable, the transverse force varies along the cable width direction. This results not only in a difference in mechanical stability [15], but also in variations in transverse stress susceptibility between the edges and the center of the cable. Pasztor *et al* [16] presented that the thin-edge exhibited 15% more critical current reduction than the center in a bare bronze-processed Nb₃Sn Rutherford cable at 160 MPa at 4.2 K, 11.5 T. After filling with solder, the variation in reduction decreased to 3%. The critical current reduction at the cable’s thin-edge decreased from 35% to 16% as well.

Over the following years, more production processes like ‘Internal-Tin (IT)’ [17], ‘Modified Jelly-Roll (MJR)’ [18], ‘Powder-In-Tube (PIT)’ and ‘Restacked-Rod-Process (RRP)’ were developed for manufacturing multi-filamentary superconducting wires with a much better non-copper critical current density performance. Obviously, examination of the transverse stress susceptibility of Rutherford cables made of these Nb₃Sn wires was needed.

To reduce the transverse stress susceptibility of Nb₃Sn type Rutherford cables, a complete and perfect epoxy resin impregnation is essential in order to create a quasi-hydrostatic pressure on the Nb₃Sn wire instead of a point like charge. Boschman *et al* [19] compared the critical current performance of a key-stoned cable with a rectangular cable. Both cables were manufactured using PIT wires. For key-stoned cables, only the outer surface was covered with Stycast 2850 FT epoxy resin, while the rectangular cable was fully impregnated. About 30% reduction in critical current appeared in the fully impregnated cable sample at 160 MPa, 4.2 K, 11 T, while

a severe reduction of 80% was found in the cable sample with partial impregnation.

The investigations on transverse stress susceptibility mentioned above are based on the method by which the ratio of the critical currents measured at applied transverse pressure and at 'zero'-stress are compared. Another method, which is a more accurate representation of the actual physical process, refers to the reversible degradation as the difference between the irreversible reduction $\Delta I_c = I_c(0 \rightarrow \sigma \rightarrow 0) - I_c(0)$ and the normalized critical current reduction $I_c(\sigma)/I_c(0)$. A quantitative investigation by Van Oort *et al* [20] on the transverse stress susceptibility of Rutherford cables manufactured with different types of Nb₃Sn wires, i.e. MJR, IT and PIT, indicated that the reversible critical current reduction and irreversible critical current degradation due to transverse stress, varies in Rutherford cables with different strand-type and cable-layout, and is difficult to predict. Other relevant researches to determine the reversible and irreversible critical current reduction of different types of Nb₃Sn cables were presented in [21–26].

Here the critical current performance of state-of-the-art Nb₃Sn Rutherford cables subjected to a magnet relevant level of transverse pressure are presented. The cables were manufactured using the cabling machine at CERN with RRP wire from Bruker-OST and PIT wire from Bruker-EAS. All measurements on wire and cable samples were carried out in boiling liquid helium at 4.2 K, focusing on seven aspects: (1) critical current of witness wires and cable samples as function of transverse magnetic field; (2) RRR of the stabilizing copper matrix at 20 K; (3) transverse pressure susceptibility in a background magnetic field of 10 T; (4) comparison of the upper critical field with and without transverse stress; (5) effect of a thermal cycle; (6) load-cycling on the critical current; and finally (7) microscopic analysis of sample cross-sections thereby checking for the presence of visible voids and filament damage.

2. Experimental details

2.1. Sample characteristics

Seven samples of different Nb₃Sn Rutherford type cables and their witness wires were measured in the cable press facility at the University of Twente. One key-stoned cable sample comprising 40 strands of RRP-108/127 and two PIT-114 cable samples are representative for the cable layout used in the so-called Dispersion Suppression (DS) demonstrator dipole magnet studies at CERN. Cable sample DS-PIT-I also comprises a 25 μm thick stainless-steel core for increasing the inter-strand resistance in the cable to reduce the coupling current loss. Cable samples DS-RRP and DS-PIT-II have no core. Four samples of the rectangular cable comprising 18 RRP-132/169 and PIT-192 strands are representative for the cables used in the Short Model Coil (SMC) racetrack type demonstrator magnets at CERN. Characteristics of cables and corresponding Nb₃Sn wires are listed in tables 1 and 2. All cable samples were vacuum impregnated with epoxy resin to enhance their mechanical properties, i.e. Araldite of CIBA GEIGY and CTD-101K in combination with glass-fibers.

2.2. Sample preparation

For sample preparation, the Nb₃Sn Rutherford cables are bent around a U-shape reaction heat treatment cable holder with bending radius of 10 mm following the wind-and-react technology [27]. Next, the cable with a virgin witness wire wound around an ITER-type barrel [28] and two straight samples used for RRR measurements, are heat treated following the recipe in table 3. When completed, the cable samples are carefully removed from the reaction holder and transferred to a comparable 'hair-pin' sample holder covered with Kapton tape for electrical insulation. Several pairs of voltage taps are soldered to the edges of the cable. As seen in figure 1, underneath the two extra layers of glass-fiber tape is the sample, which is fixed on a U-shape sample holder. The two extra layers of glass-fiber tape are used to increase the thickness of the cured epoxy at the loading area (on the left side of the view). A Teflon block is temporarily placed covering the loading area of the cable and to also apply a bit of pre-stress and guide the liquid epoxy during the vacuum impregnation. Next, a Kapton tape is glued to the surface of the Teflon block in contact with the cable. This step is performed to provide a smooth interface to the impregnated cable. In addition, three straps of glass-fiber tape are applied to each side of the straight legs of the U-shape sample holder to mechanically fix the cable to the sample holder. A PT100 temperature sensor and two resistive heaters are present for controlling the temperature of the sample holder during vacuum impregnation and curing.

Two preparation methods for Nb₃Sn Rutherford cable samples for transverse stress measurements are in use as shown in figure 2. The DS cables exhibit a keystone angle of 0.75° for RRP cable and 0.71° for PIT cable and are wrapped with glass-fiber tape with 50% overlap as shown in figure 2(a). The SMC Rutherford cables are prepared as shown in figure 2(b), which is representative for coil impregnation. Cable sections were first inserted into a glass-fiber sleeve where after a stack of two cable units were wrapped again with a glass-fiber tape with 50% overlap. A dummy cable is used to transfer pressure to the measured sample placed on the top.

The DS cable samples were impregnated with Araldite epoxy resin mixture MY740/HY906/DY062 of CIBA GEIGY [29, 30]. This epoxy resin system, see table 4, was used before for the impregnation of Nb₃Sn coils [31–34], and features a pot life of 6 h at the processing temperature of 55 °C.

However, epoxy resin for coil application requires a long pot life and low viscosity. CTD-101 K [35], see its characteristics in table 4, has a very low viscosity of 400 mPa s and long pot life of 60 h. For this reason, it is nowadays regularly used for vacuum impregnation of large coils for accelerator magnets [35]. Nb₃Sn cables SMC-RRP and SMC-PIT were impregnated using this epoxy resin. Araldite and CTD-101K epoxy resins have a thermal contraction of more than 1.1% from room temperature to 4.2 K, a value too big in comparison to heat treated Nb₃Sn Rutherford cables of 0.3% from room temperature to 4.2 K [36]. For this reason, S-2 glass-fiber sleeve is used to decrease the thermal contraction values of the epoxy resin.

Table 1. Characteristics of the Nb₃Sn Rutherford cables investigated for their Transverse Stress Susceptibility.

Parameter	DS-RRP	DS-PIT-I	DS-PIT-II	SMC-RRP	SMC-PIT
Cable identifier	—	H15EC0126AB	H15EC0126AC	H03EC0120A	H03EC0140A
Width/mid-thickness (mm)	14.70/1.25	14.70/1.25	14.70/1.25	9.97/1.81	9.93/1.81
Type of strand process	RRP-108/127	PIT-114	PIT-114	RRP-132/169	PIT-192
Core material if present	—	SS 316L	—	—	—
Core size <i>w/t</i> (mm)	—	12/0.025	—	—	—
Number of strands	40	40	40	18	18
Keystone angle (°)	0.75	0.71	0.71	0	0
Transposition length (mm)	100	100	100	63	63
Number of samples	1	1	1	2	2

Table 2. Characteristics of the strands in the Nb₃Sn Rutherford cables samples.

Property/Wire	RRP-108/127	PIT-114	RRP-132/169	PIT-192
Wire diameter D_{wire} (mm)	0.700	0.700	1.000	1.000
Filament diameter $D_{filament}$ (μm)	55	43	58	48
Cu/non-Cu ratio	1.13	1.33	1.22	1.22

Table 3. Heat treatment protocols used for the Nb₃Sn Rutherford cables.

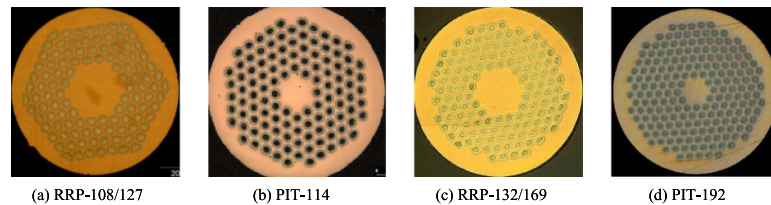
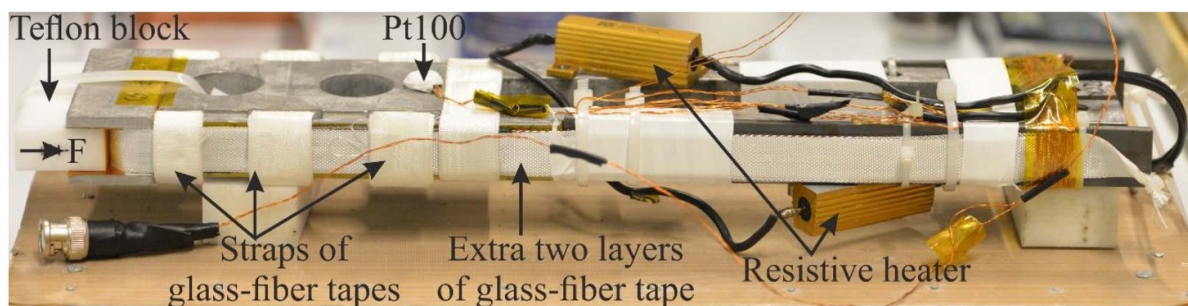
Property/Project	RRP-108/127	PIT-114	RRP-132/169	PIT-192
Final HT step	50 h at 650 °C ^a	200 h at 625 °C ^b	50 h at 665 °C ^c	120 h at 640 °C ^d
Ramp rate	5 °C h ⁻¹	50 °C h ⁻¹	50 °C h ⁻¹	50 °C h ⁻¹

^aIntermediate temperature plateaus: 48 h at 210 °C, ramp 5 °C h⁻¹ and 48 h at 400 °C, ramp 5 °C h⁻¹.

^bIntermediate temperature plateau: 100 h at 600 °C, ramp 50 °C h⁻¹.

^cIntermediate temperature plateaus: 72 h at 210 °C, ramp 25 °C h⁻¹ and 72 h at 400 °C, ramp 50 °C h⁻¹.

^dIntermediate temperature plateau: 100 h at 620 °C, ramp 50 °C h⁻¹.

**Figure 1.** Nb₃Sn U-shaped sample prepared for vacuum impregnation.**Figure 2.** Sketch of Nb₃Sn Rutherford cable cross-sections in the force loaded area. (a) DS Rutherford cables; (b) SMC Rutherford cables; (c) Longitudinal section views of sample holder and side plate.

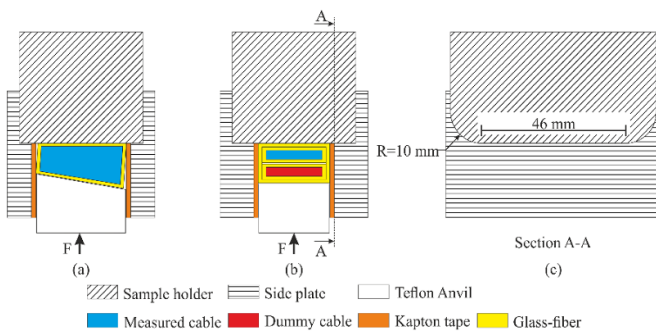
To apply a uniform force over the pressure area during the transverse pressure measurement is essential. Therefore, a proper alignment of pushing block and pressure surface is crucial. The vacuum impregnation of the sample itself on the ‘hair-pin’ sample holder with the Teflon block

as ‘placeholder’, cannot ensure that the surface is perfectly aligned with the actual pushing block.

Any misalignment of the pushing block will result in a non-uniform stress distribution along the impregnated cable. To warrant the alignment of the pushing anvil and cable surface,

Table 4. Characteristics of epoxy resin used for the impregnation of Nb₃Sn cable samples [29, 30, 35].

Parameter/Epoxy	MY740/HY906/DY062	CTD-101 K
Viscosity (mPa s)	12 000/175–225/≤10 (at 25 °C)	400 (at 40 °C)
Density (g cm ⁻³)	1.16/1.14/0.90 (at 25 °C)	1.03 (at 25 °C)
Mixing ratio in mass	100/90/0.2	Part A:Part B:Part C = 100:90:1.5
Pot life	6 h at 55 °C	60 h at 40 °C
Curing schedule	4 h at 85 °C + 16 h at 110 °C	5 h at 110 °C + 16 h at 125 °C

**Figure 3.** Schematic of the alignment impregnation performed to guarantee uniform force distribution of the pressure block onto the sample surface.

an additional impregnation is applied, see figure 3 [37, 38]. Two layers of glass-fiber tapes brushed with degassed Stycast 2850 FT/23LV are added to the impregnated cable. A layer of Kapton tape is glued onto the bottom surface of the anvil as well as the inside faces of the two clamping plates. The anvil is positioned by two spark-eroded plates fixed to the sample holder by two pins. After the epoxy resin has cured, the side plates and stainless-steel strips are removed. This recipe ensures that the anvil is well aligned to the pressed section of the sample holder. The transverse pressure can now be applied uniformly on the impregnated cable sections.

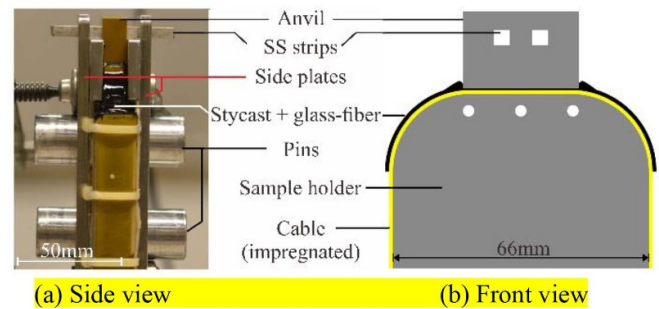
Once impregnated, the sample is connected to the superconducting transformer for generating the sample current. The total joint resistance between sample and transformer terminals needs to be as low as possible, since it determines how long a steady test current can be maintained [23]. Tin-silver 96Sn4Ag with 221 °C melting temperature is applied. The joint is covering one transposition length of the cables as shown in figure 4. Glass-fiber tape straps soaked in Stycast and cured, are used to fix the splice. The joint resistance is calculated from the measured current decay time constant of the secondary closed loop and listed in table 5. All values are smaller than 10 nΩ, and retain a relatively low level.

2.3. Measurement setup

The measurement setup for characterization of the transverse stress effect on superconducting cables at the University of Twente consists of a superconducting transformer injecting the sample current and an electro-magnetic press generating the transverse force exerted on the cable surface [23, 39]. The primary current of the transformer can be swept from -50 A to +50 A, thereby introducing a current of 100 kA maximum

Table 5. Total joint resistance comprising two splices between cable sample and secondary coil.

Cable sample	Total joint resistance (nΩ)
DS-RRP	3.0 ± 0.5
DS-PIT-I	3.0 ± 0.2
DS-PIT-II	6 ± 1
SMC-RRP-I	3.5 ± 1.0
SMC-RRP-II	3.0 ± 0.5
SMC-PIT-I	3 ± 1
SMC-PIT-II	2.0 ± 0.1

**Figure 4.** ‘Hair-pin’ sample holder showing the position of the two joints of the Nb₃Sn Rutherford cable sample connecting to the terminals of the transformer secondary coil. The pressed area is on the left side of the picture.

in the secondary coil and thus in the connected sample. The mechanically loaded section of the sample is situated in an 11 T solenoid at 4.2 K, as shown in figure 5 [23]. The magnetic field inside the bore is from bottom to top of the magnet. To minimize the effect of the Lorentz force in the cable sample generated when injecting the current, two measures are applied: (1) the injection current in the cable sample generates a Lorentz force pointing to the thick side of the sample; (2) training quenches were applied several times for each measurements until the quench current reached a stable value. At this moment, a close connection between the side plate and the thick-side of cable sample is considered.

The electro-magnetic press consists of two anti-series connected and repelling NbTi flat coils as shown in figure 5 [23]. The top coil pushes the pressure anvil against the sample via a piston while the bottom coil connects to the sample holder by a thick steel sleeve and fixation pins. A maximum force of 250 kN can be exerted onto the cable surface over a length of 45 mm for the DS Nb₃Sn Rutherford cables and 46 mm for the SMC cables. The force is determined by two independent

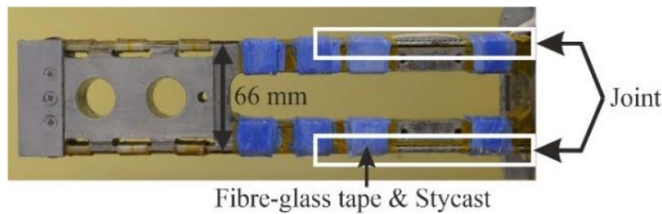


Figure 5. Schematic longitudinal section of the electromagnetic cryogenic cable press, sample holder and main solenoid (with an upward magnetic field inside the bore) [38].

methods [39]. The displacement of the upper coil is measured with an extensometer; and two strain gauges on the pressure anvil allow to monitor the deformation.

3. Estimate of measuring errors

When determining the critical current of the Nb_3Sn under transverse pressure, we compare the critical current value at a given pressure to the value measured under no-load condition. To determine the onset of irreversible degradation, it is essential to estimate the possible error in the measured critical current value and these can be classified either as random or systematic [40].

For the critical current, the random error comprises the resistive slope correction of 0.5% to 1%, the quality of the power-law fit of the corrected $E-I$ curve of 0.3% and pressure fluctuations in the closed helium recovery system of 0.1%. The systematic error comprises the instrumental calibration and offset of 1.5%, uncertainty in the voltage tap position of 0.1% and the uncertainty in peak magnetic field of some 2% to 4%. Adding up these contributions, we estimate a systematic error of maximum 5% and a random error of 1.5% in the I_c -values. The corresponding error estimates are summarized in table 6 and details of this analysis were reported in [41].

This latter estimate has a direct impact on the determination of the irreversible pressure limit. At this point, filaments start to crack and the critical current degrades irreversibly. Like for single-strand experiments reported in [42], this is detected by cycling the transverse pressure back to a reference critical current at a low stress value, repeating the low-stress critical current measurement and comparing the outcome to its earlier value. For an observed reduction in critical current to be significant, it has to be larger than the random uncertainty of 1.5%. Hence, in section 4 the criterion for determining the irreversible pressure limit is set as the pressure that causes an irreversible critical current reduction of 2%.

To determine the error in the transverse pressure a different approach was taken. Rather than estimating different contributions *a-priori*, e.g. the friction acting on the force transmitting piston in figure 5, two independent methods are compared to measure the pressure and the difference used for estimating the error.

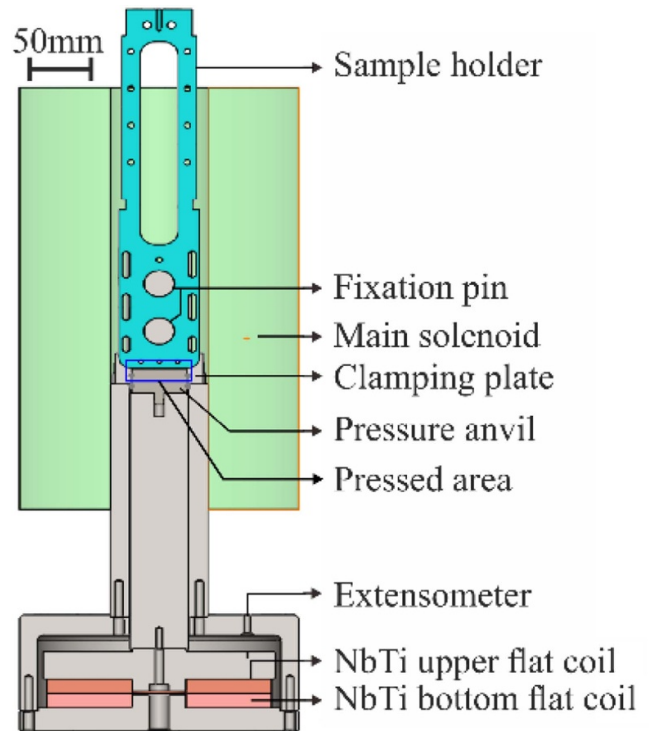


Figure 6. Transverse stress calculated from the strain gauges, plotted against the transverse stress calculated from the current in the press and displacement of the upper press coil detected by the extensometer. The two colors correspond to the two different strain gauges on either side of the pressure anvil.

The pressure exerted on the cable can be derived by simply dividing the force with which the two NbTi force-driving coils repel by the surface area of the pressure anvil. The force is calculated from the current with which the coils are excited, their dimensions and their distance. By measuring the distance with an extensometer and factoring in a correction due to the interaction between the electromagnetic press and the main magnet [43], the force is calculated with an error of 2% [39]. The second method for measuring the pressure is to monitor the deformation of the steel pressure anvil with two strain gauges with an error of 3% [39].

If the force exerted by the press coils is transmitted frictionless to the anvil and balanced there by the reaction force in the sample, plotting the two pressure measurements will yield a curve with unit slope. Such a curve is indeed observed in figure 6 for the SMC-RRP-II cable. In most cases some deviation occurs between the force-derived pressure value and the one determined from the strain gauge readings, e.g. for the DS cables shown in figure 6. We use the average intercept of the curves, one for each gauge, with the x -axis as an estimate for the error in the applied pressure. From figure 6, the estimate is 3 MPa for cable sample SMC-RRP-II and 10 MPa for cable sample DS-PIT-I. In view of the observed linearity of the curves, we take this error as systematic within a measurement run.

Table 6. Estimated errors in the critical current measurement under transverse pressure conditions.

Source	Type, random or systematic	Relative error (%)
Instrumental calibration and offset	Systematic	1 to 1.5
Resistive slop correction	Random	0.5 to 1
Uncertainty voltage tap position	Systematic	0.1
E–I power law fit/extrapolation	Random	0.3
Uncertainty bath temperature	Random	0.1
Uncertainty peak field value	Systematic	2 to 4
Total systematic error assumed		5
Total random error assumed		1.5

Table 7. Estimated errors in the transverse pressure.

Cable sample	Error in pressure (MPa)
DS-RRP ^a	±12
DS-PIT-I ^a	±10
DS-PIT-II ^a	±30
SMC-RRP-I ^a	±32
SMC-PIT-I ^a	±23
SMC-RRP-II	±3
SMC-PIT-II	±3

^aCable samples not prepared with an alignment impregnation.

The error analysis for all measurements is presented in next section 4 and reported in table 7.

4. Results

4.1. Critical current of witness wires and cables

In order to compare the critical currents of wire and cable samples directly, it is customary to report the critical current as function of the peak magnetic field B_{peak} , the maximum value of the total magnetic field experienced by the superconducting filaments. For a wire sample on the sample holder, the position of the peak field is at the outer edge of the filamentary zone and the self-field correction is made using the widely used formula [44]

$$\begin{aligned} B_{\text{peak, wire}} &= B_a + B_{\text{sf, wire}} \\ &= B_a + \left(\frac{\mu_0}{2\pi R} - 0.09 \right) I_{\text{wire}} \times 10^{-3}, \end{aligned} \quad (1)$$

where $B_{\text{sf, wire}}$ in tesla is the self-field of the wire, μ_0 in H/m is the magnetic permeability of vacuum, R in mm is the radius of the filamentary zone, and I_{wire} in ampere is the current in the sample. This formula is valid only when the Lorentz force pushes the sample onto the barrel. The first term represents the self-field of a straight wire and the second is a correction of the self-field taking in account the helical shape of the sample. The value of R is 0.29 mm for PIT-114, 0.4 mm for RRP-132/169 and 0.42 mm for PIT-192 wire samples estimated using the cross-section views of the virgin wires shown in figure 7.

For a cable, a 2D electromagnetic COMSOL model was developed to estimate the peak magnetic field in the filaments yielding a self-field correction of

$$B_{\text{peak, cable}} = B_a + \eta \times I_{\text{cable}}, \quad (2)$$

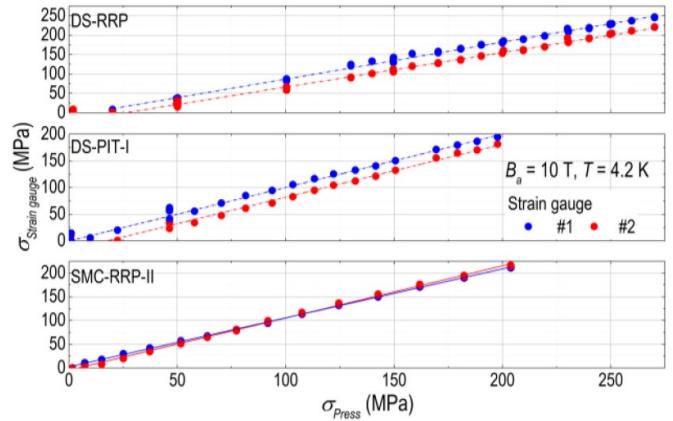


Figure 7. Cross-sections of four Nb₃Sn wires: (a) RRP-108-127 wire with 0.7 mm diameter; (b) PIT-114 wire with 0.7 mm diameter; (c) RRP-132/169 wire with 1 mm diameter; (d) PIT-192 wire with 1 mm diameter [45, 46].

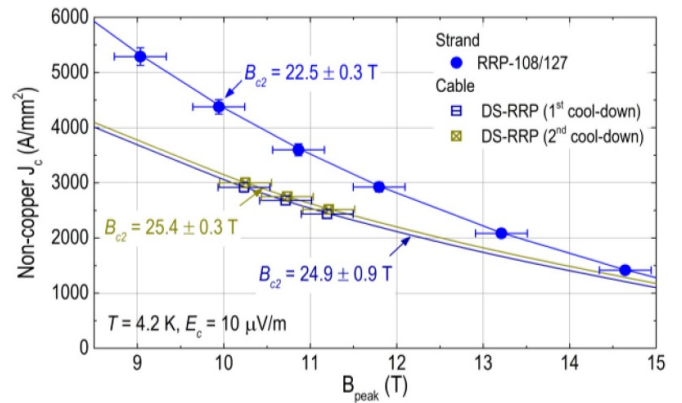
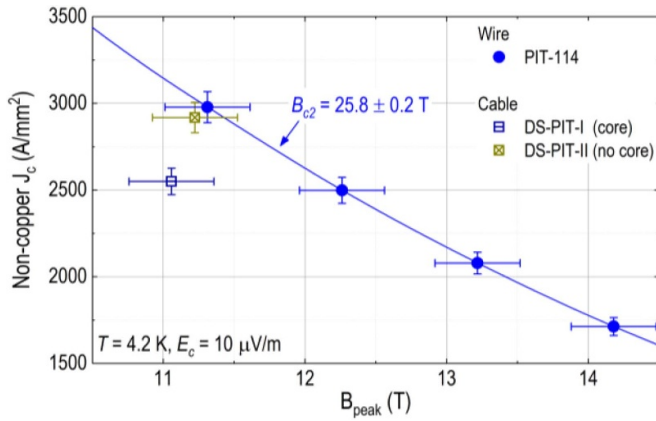


Figure 8. Non-copper critical current density of the DS-RRP witness wire (circles), plotted against the peak magnetic field on the superconductor. Discrete symbols represent the measured data, and the solid line is a fit of the data following the Kramer like equation (5). Also indicated are the upper critical field B_{c2} values that result from the fits. For comparison, non-copper J_c values of the DS-RRP cables (squares) are also included in the graph, measured at low-level stress in the $I_c(\sigma)$ campaign. The error bars in critical current density and peak magnetic field are systematic errors of 3% and 0.3 T, respectively.

where I_{cable} is the current flowing in the sample and η is 0.056 mT A⁻¹ for the DS-RRP cable sample, 0.061 mT A⁻¹

Table 8. Kramer extrapolation for finding the upper critical field B_{c2} and the non-copper critical current density J_c (4.2 K, 12 T) of the various witness wires and cables, obtained by fitting expression [47] to the measured data.

		B_{c2} (T)	J_c (4.2 K, 12 T) ($A\ mm^{-2}$)
DS-RRP wire and cables			
Wire	RRP-108/127	22.5 ± 0.3	2810 ± 85
Cable	DS-RRP (1st cool-down)	24.9 ± 0.9	2090 ± 60
	DS-RRP (2nd cool-down)	25.4 ± 0.3	2170 ± 65
DS-PIT wire			
Wire	PIT-114	25.8 ± 0.2	2620 ± 80
SMC-RRP wires and cables			
Wire	RRP-132/169 (CERN)	26.6 ± 0.4	3200 ± 190
	RRP-132/169 (UT strand1)	26.2 ± 0.3	3180 ± 190
	RRP-132/169 (UT strand2)	26.2 ± 0.3	3100 ± 190
Cable	SMC-RRP-II (1st cool-down)	26.4 ± 1.1	3120 ± 190
	SMC-RRP-II (3rd cool-down)	25.4 ± 1.1	3080 ± 185
SMC-PIT wires and cable			
Wire	PIT-192 (UT strand1)	26.1 ± 0.4	2490 ± 150
	PIT-192 (UT strand2)	26.0 ± 0.4	2460 ± 150
Cable	SMC-PIT-II	24.3 ± 0.6	2520 ± 150


Figure 9. Non-copper critical current density of the DS-PIT witness wire (circles), plotted against the peak magnetic field on the superconductor. The discrete symbols represent the measured data, and the solid line is a fit of the data following the Kramer like equation (5). Also indicated is the upper critical field B_{c2} value that results from the fit. For comparison, non-copper J_c values of the DS-PIT cables (squares) are also included in the graph, measured at low-level stress in the $I_c(\sigma)$ measurement campaign. The error bars on the critical current density and peak magnetic field are systematic errors of 3% and 0.3 T, respectively. Note that no $J_c(B)$ values of the DS-PIT cables were measured.

for the DS-PIT cable samples and $0.078\ mT\ A^{-1}$ for the SMC-RRP and SMC-PIT cable samples.

For further ease of a direct comparison between wire- and cable data, ‘non-copper’ critical current density values $J_{c,wire}$ are reported. For a wire, this value is calculated following

$$\text{Non - copper } J_{c,wire} = \frac{I_{c,wire}(1 + \varsigma)}{A_{wire}}, \quad (3)$$

where $I_{c,wire}$ in ampere is the measured wire critical current, A_{wire} in mm^2 is the wire’s cross-sectional area and ς is its Cu to non-Cu ratio as listed in table 1. In the case of a cable, $J_{c,cable}$

is calculated following

$$\text{Non - copper } J_{c,cable} = \frac{I_{c,cable}(1 + \varsigma)}{N * A_{wire}}, \quad (4)$$

where $I_{c,cable}$ in ampere is the cable’s measured critical current and N is the number of strands listed in table 2. For reference, the $J_c(B_{peak})$ curves are also fitted to a commonly used variation of the Kramer expression [47]

$$\text{Non - copper } J_c(B_{peak}, T) = \frac{C}{B_{peak}} \times B_{c2}(T)^2 \times h^p(1 - h)^q, \quad (5)$$

$$h = \frac{B_{peak}}{B_{c2}(T)}, \quad (6)$$

where C in $A\ (mm^{-2}\ T^{-1})$ is a fitting constant, $B_{c2}(T)$ is the upper critical field, p and q are the low- and high-field exponents of the pinning force for a specific wire, respectively. In the Kramer extrapolation, p and q are fixed at 0.5 and 2 [48], respectively. The fit curves are added to the $J_c(B_{peak})$ graphs here below and the fit parameters are reported in table 8.

4.1.1. DS Nb_3Sn wire and cables. The magnetic field dependent critical current densities of the RRP-108/127 and PIT-114 Nb_3Sn wires used for the cables in Dispersion Suppression magnets are shown in figures 8 and 9, respectively. The critical current density points of cable sample DS-RRP, DS-PIT-I with a stainless-steel core and DS-PIT-II without core, are added to the graphs for comparison. The critical current of the cables was also measured when exposed to transverse pressure, as reported in section 4.1.2. The $I_c(\sigma)$ measurements were carried out in a background magnetic field of 10 T and the relevant non-copper J_c were determined at the low-level pressure of 1.5 MPa for cable sample DS-RRP, 3 MPa for cable sample DS-PIT-I and 2 MPa for cable sample DS-PIT-II. The non-copper J_c values of DS-RRP witness wire at

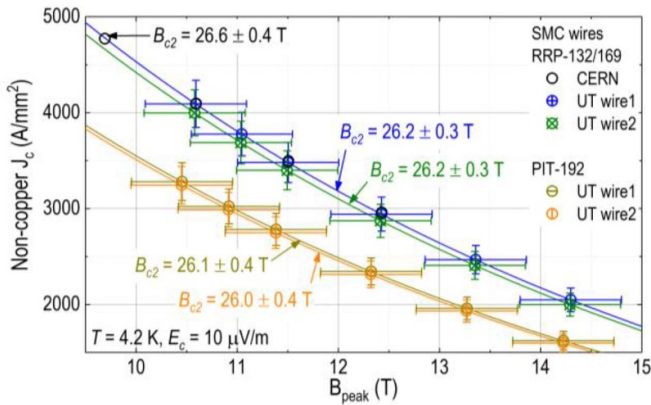


Figure 10. Non-copper critical current density of the SMC witness wire, plotted against the peak magnetic field on the superconductor. The discrete symbols represent the measured data, and the solid lines are fits of the data following the Kramer like equation (5). Also indicated are the upper critical field B_{c2} values that result from the fits. The topmost three curves correspond to RRP-132/169 wire samples. For comparison, an independently measured data set recorded at CERN is included in the plot. The two lower curves correspond to PIT-192 wire samples. The error bars on the critical current density and peak magnetic field are based on 6% and 0.5 T systematic errors, respectively.

11.0 ± 0.3 T are 3480 ± 100 A mm $^{-2}$, while for the corresponding cable sample during the first and second cool-down 2540 ± 80 A mm $^{-2}$ and 2640 ± 80 A mm $^{-2}$ were found, respectively. The deviation in J_c values at 11.0 ± 0.3 T between the witness wire and cable samples is larger than 25% and unlikely caused by measurement uncertainties. It can be indicative of performance degradation due to cabling or thermal stress resulting from impregnation. Also, no significant deviation of cable J_c from one cool-down to the next was observed.

In addition, the critical current density is 2480 ± 75 A mm $^{-2}$ at 11.1 ± 0.3 T and 2860 ± 85 A mm $^{-2}$ at 11.2 ± 0.3 T for cable samples DS-PIT-I and DS-PIT-II, respectively. Given the 3% systematic error in the critical current as described in section 2, a significant non-copper J_c degradation of some 20% was observed in cable sample DS-PIT-I when compared to the wire sample in the same magnetic field. No significant degradation was observed in cable sample DS-PIT-II. It is concluded that the cabling of the PIT-114 wires caused about 20% critical current degradation in cable sample DS-PIT-I, but no reduction in cable sample DS-PIT-II.

4.1.2. SMC Nb $_3$ Sn wire and cables. In figure 10 the non-copper $J_c(B)$ behavior of two types of Nb $_3$ Sn wires used for the SMC cables are compared. Two RRP-132/169 and two PIT-192 witness wires were heat treated independently and measured at the University of Twente. For comparison, the non-copper J_c of a third RRP-132/169 virgin wire prepared, heat treated and measured at CERN [21] is included in the graph.

The three RRP-132/169 wire samples behave in a very similar way. Their differences in critical current density fall within the 6% systematic error, and are thus not significant. The critical current density at 12 T is 3200 ± 190 , 3180 ± 190

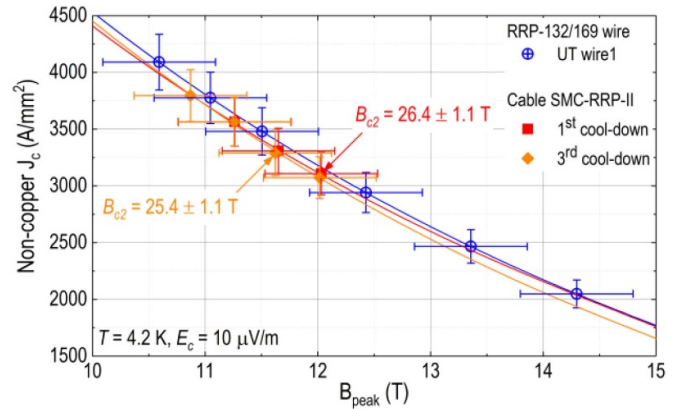


Figure 11. Non-copper critical current density of the SMC-RRP witness wire (circles) and cable (squares and diamonds), plotted against the peak magnetic field on the superconductor. The discrete symbols represent measured data, and the solid lines are fits of the data following the Kramer like equation (5). Also indicated are the upper critical field B_{c2} values that result from these fits. The wire sample data are repeated from figure 10. The two sets of cable data are obtained on the same sample, but in different cool-down runs. The error bars on the critical current density and peak magnetic field are systematic errors of 6% and 0.5 T, respectively.

and 3100 ± 190 A mm $^{-2}$ for ‘CERN’, ‘UT wire1’ and ‘UT wire2’ RRP-132/169 wire samples, respectively. This result has increased confidence in both sample-to-sample and lab-to-lab reproducibility of the measurements, as well as in the level of quality control mastered by the wire manufacturer. A similar conclusion can be drawn for the PIT-192 witness wire samples as no significant difference in the critical current density between the two PIT wire samples is observed. The non-copper J_c values at 12 T are 2490 ± 150 and 2460 ± 150 A mm $^{-2}$ for ‘UT wire1’ and ‘UT wire2’ samples, respectively.

When comparing the SMC-RRP- and PIT wire samples, it is concluded that both Nb $_3$ Sn wire-manufacturing processes yield the same average B_{c2} values, but the PIT wire samples have an average non-copper J_c at 12 T about 15% lower than in the RRP wire samples taking into account the 6% systematic error.

When comparing the non-copper $J_c(B)$ values of cables samples SMC-RRP and -PIT with corresponding witness wires, only cable samples SMC-RRP-II and -PIT-II were measured.

In figure 11 the non-copper $J_c(B)$ values of cable sample SMC-RRP-II and RRP-132/169 wire sample ‘UT wire1’ are compared. The two data sets of sample SMC-RRP-II correspond to different cool-down cycles.

Differences in performance between wire samples and cable samples are minor. The average B_{c2} of cable sample SMC-RRP-II is 25.9 ± 1.1 T. When comparing to the average B_{c2} of the three wire samples of 26.3 ± 0.3 T, the deviation is still within the estimated uncertainty and no significant difference is observed. A similar conclusion can be drawn regarding the comparison of the non-copper J_c values between wire samples and cable samples. It is concluded that in this case there is no significant degradation by cabling. Differences both

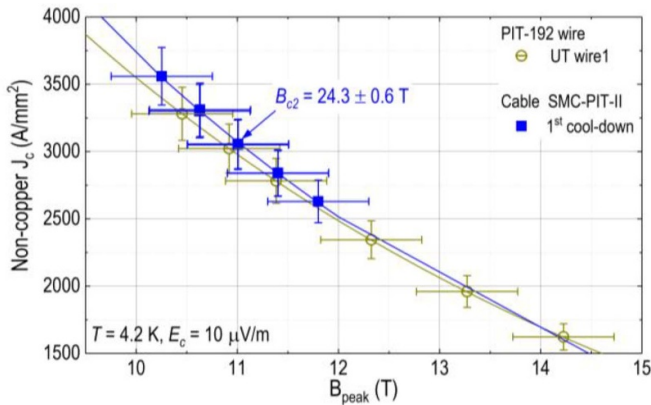


Figure 12. Non-copper critical current density of the SMC-PIT witness wire (circles) and cable (squares), plotted against the peak magnetic field on the samples. The discrete symbols represent the experimental data, and the solid lines are fits of the data following Kramer expression equation (5). Also indicated are the upper critical field B_{c2} values that result from the fits. The wire sample data are repeated from figure 10. The error bars on the critical current density and peak magnetic field are systematic errors of 6% and 0.5 T, respectively.

in upper critical field and non-copper J_c between the two cool-down runs of the cable samples are also negligible.

In figure 12 the non-copper $J_c(B)$ of cable SMC-PIT-II and of the PIT-192 virgin wire sample ‘UT wire1’ are presented. The upper critical field of the cable is about 5% lower than the average value found in the wire samples, but their critical current density values within the measurement range are similar when taking into account the 6% systematic error. It is concluded that the cabling process has no significant influence on the current-carrying capacity of the material.

For ease of reference, all fitted B_{c2} and $J_c(4.2\text{ K}, 12\text{ T})$ values discussed above are summarized in table 8.

The thermal- and electrical conductivities of the stabilizing copper in high- J_c Nb_3Sn strands are important parameters for the stability of a superconducting magnet [49]. The copper conductivity at liquid helium is quantified by the RRR value by which a larger RRR means a larger conductivity of the copper. An adequate stabilizer for accelerator magnet features an RRR (273.15 K/4.2 K) in excess of 100 [50]. Therefore, the RRR of the virgin wire and extracted strand samples of RRP-132/169 and PIT-192 samples were measured as well and the results are presented in table 9.

Table 9 indicates that all measured SMC samples have an adequate copper stabilizer. The measured RRR values for virgin wire samples of cable SMC-RRP-I and cable SMC-PIT-I are reproducible within 10%, and 20% for cable SMC-RRP-II. No RRR reduction was found in the extracted strands in comparison to the virgin wires of cable SMC-RRP-I, but up to 40% RRR degradation was observed in the extracted strands of cable SMC-RRP-II. One of the measured extracted strands of cable SMC-PIT-I shows a maximum of 30% RRR reduction, while the other one performs similar to the virgin wires. The significant differences are not caused by measurement errors,

and a possible explanation is that the extracted strand samples were taken from the ends of cable sample, where the cable was bent. Any damage of the diffusion barrier can cause a decrease of the RRR value. Nevertheless, the RRR values of virgin wire and extracted strand samples fulfill the magnet design requirement. Since the $J_c(B)$ of the SMC-RRP cables performs identical to the virgin wires, no critical current degradation due to cabling was observed. The relatively low RRR values of the extracted strands of cable samples SMC-RRP-II and SMC-PIT-I are considered not representative.

4.2. Irreversible I_c degradation

A typical run of measurements consists of measuring the critical current of the sample at a discrete number of gradually increasing transverse stress. After each measurement, the stress on the cable is released and the critical current at ‘zero’-stress is determined. A light pressure is always maintained to prevent various parts in the set-up from losing contact and shifting. The value is compared to the initial critical current at ‘zero’-stress, so that possible irreversible I_c -reduction due to the earlier pressure excursion can be detected and quantified.

4.2.1. DS Rutherford cable. The initial critical current of sample DS-RRP at 4.2 K and a peak magnetic field of $11.2 \pm 0.3\text{ T}$ is $21.7 \pm 0.7\text{ kA}$. The initial critical current of sample DS-PIT-I with a stainless-steel core at the peak field of $11.1 \pm 0.3\text{ T}$ is $17.1 \pm 0.5\text{ kA}$, and for DS-PIT-II at the peak field of $11.2 \pm 0.3\text{ T}$ it is $19.8 \pm 0.6\text{ kA}$. The critical current performance of the three cables with respect to transverse pressure is shown in figure 13. All cables display a relatively steep $I_c(\sigma)$ dependence, falling to 90% of their unstressed value at $250 \pm 12\text{ MPa}$ for sample DS-RRP; at $100 \pm 10\text{ MPa}$ for sample DS-PIT-I; and at $70 \pm 30\text{ MPa}$ for sample DS-PIT-II. The onset of irreversible critical current reduction is observed at $250 \pm 12\text{ MPa}$ for sample DS-RRP; at $90 \pm 10\text{ MPa}$ for sample DS-PIT-I; and $70 \pm 30\text{ MPa}$ for sample DS-PIT-II taking into account the 1.5% random error in the critical current measurement and using 2% reduction of the critical current measured at ‘zero’-stress as the criterion, as motivated in section 3.

4.2.2. SMC Rutherford cables. In the case of cables SMC-RRP and SMC-PIT, similar $I_c(\sigma)$ measurements were carried out on two samples for each type of cable. Cable samples SMC-RRP-I and SMC-PIT-I were vacuum impregnated with CTD-101K. Cable samples SMC-RRP-II and SMC-PIT-II were also first impregnated with CTD-101K, but then an additional ‘alignment’ impregnation was applied, as described in section 2, in order to reduce the interface misalignment between anvil and cable surface, which was observed in the impregnated samples SMC-RRP-I and SMC-PIT-I. The $I_c(\sigma)$ behavior of samples SMC-RRP-II and SMC-PIT-II are reported first in figure 14. Their no-load initial I_c is $21.1 \pm 1.3\text{ kA}$ for SMC-RRP-II and $18.2 \pm 1.1\text{ kA}$ for SMC-PIT-II. 90% of the no-load I_c value is reached at $130 \pm 3\text{ MPa}$ for SMC-RRP-II and at $90 \pm 3\text{ MPa}$ for sample SMC-PIT-II. The onset of

Table 9. RRR of virgin wires and extracted strand samples of SMC cables.

SMC cable	RRR (273.15 K/20 K)							
	RRP-132/169				PIT-192			
	Virgin wires		Extracted strands		Virgin wires		Extracted strands	
	#1	#2	#3	#4	#1	#2	#3	#4
-I	138	125	148	147	178	160	122	168
-II	173	140	109	113	—	—	—	—

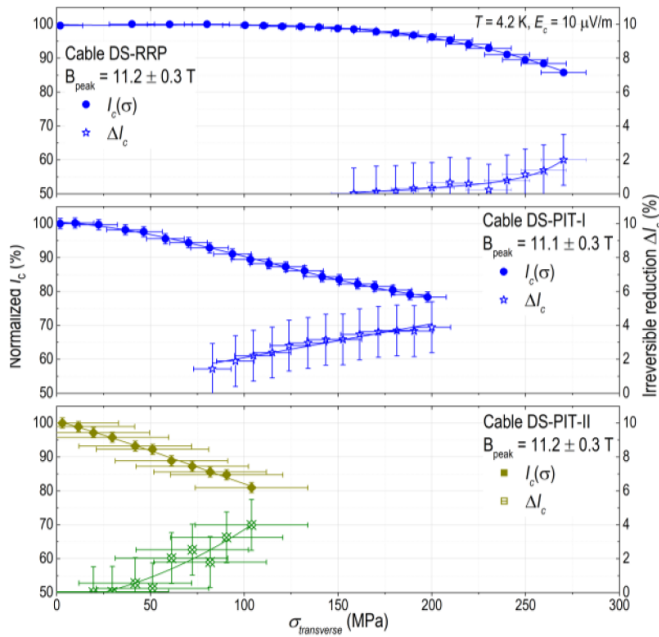


Figure 13. Transverse pressure response of the DS cables at 4.2 K at a peak magnetic field of 11.2 T on the DS-RRP cable, 11.1 T on the DS-PIT-I cable and 11.2 T on the DS-PIT-II cable. The left-hand axis corresponds to the normalized critical current $I_c(\sigma)/I_c(0)$ in percentage as function of transverse stress σ (solid symbols). The right-hand axis reports the irreversible degradation ΔI_c of the critical current with respect to its unstressed initial value (open symbols).

Table 10. Summary of the transverse stress limit for measured Nb₃Sn Rutherford cables.

Cable sample	$\sigma (\Delta I_c = -10\%)$ MPa	$\sigma (\Delta I_{c, irrev.} = -2\%)$ MPa
DS-RRP	250 ± 10	$>250 \pm 10$
DS-PIT-I	100 ± 10	90 ± 10
DS-PIT-II	70 ± 30	70 ± 30
SMC-RRP-II	130 ± 3	$>190 \pm 3$
SMC-PIT-II	90 ± 3	$>150 \pm 3$

irreversible transverse pressure is larger than 190 ± 3 MPa, and 150 ± 3 MPa for samples SMC-RRP-II and SMC-PIT-II, respectively.

For ease of reference, the measured transverse stress limits of the Nb₃Sn cables are listed in table 10.

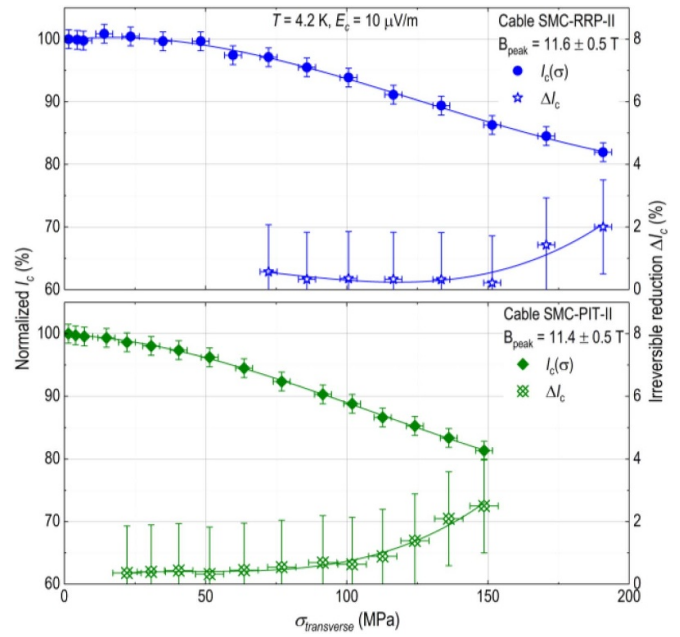


Figure 14. Transverse pressure response of the second set of SMC cables. The peak magnetic field is 11.6 ± 0.5 T for cable sample SMC-RRP-II and 11.4 ± 0.5 T for cable sample SMC-PIT-II. ‘Zero’-pressure initial currents $I_c(\sigma = 0)$ are 21.1 ± 1.3 kA for SMC-RRP-II and 18.2 ± 1.1 kA for SMC-PIT-II. Solid symbols represent the normalized critical current $I_c(\sigma)/I_c(0)$ as a function of the transverse stress σ (left axis), while open symbols are the irreversible degradation ΔI_c (right axis). The solid lines represent polynomial fits to the data. The error in the critical current is $\pm 1.5\%$; the error in the transverse pressure is ± 3 MPa for cable samples SMC-RRP-II and SMC-PIT-II.

The mentioned additional ‘alignment’ impregnation turned out to be essential for arriving at reliable transverse pressure results. In order to demonstrate what can happen when this step is omitted an erroneous measurement is presented next. The $I_c(\sigma)$ behavior of cable samples SMC-RRP-I and SMC-PIT-I with no ‘alignment’ impregnation is presented in figure 15. Note once more, that the results in this figure do not correctly show the true transverse pressure effect due to an imperfectly aligned pressure block and cable surface. Unfortunately, the critical current of cable sample SMC-RRP-I could not be measured, so instead its quench current performance as function of transverse pressure is used. It is observed that the quench and critical current decrease relatively steeply with applied pressure. The reversible critical current reaches 90% of its un-load value already at 100 ± 30 MPa for cable sample SMC-RRP-I, and at 60 ± 20 MPa for cable

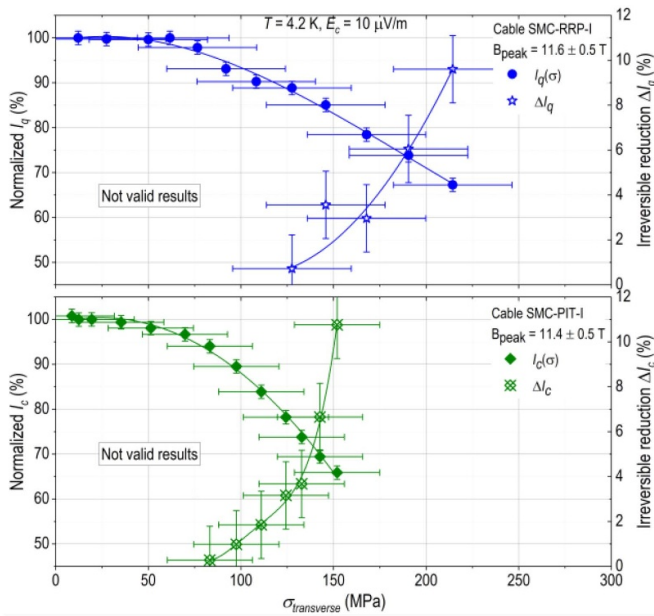


Figure 15. Erroneously measured transverse pressure response of the first set of SMC cables demonstrating that non-representative measurement results can easily be obtained when anvil and cable surface are not well aligned. The peak magnetic field is estimated at 11.6 ± 0.5 T for cable sample SMC-RRP-I, and 11.4 ± 0.5 T for cable sample SMC-PIT-I. ‘Zero’-pressure initial currents $I_q(\sigma = 0)$ are 20.7 ± 1.2 kA for SMC-RRP-I and $I_c(\sigma = 0)$ 18 ± 1.1 kA for SMC-PIT-I. Solid symbols represent the normalized $I_q(\sigma)/I_q(0)$ or $I_c(\sigma)/I_c(0)$ as function of transverse stress σ (left axis), and open symbols represent the irreversible degradation ΔI_q or ΔI_c (right axis). The solid lines represent polynomial fits of the data. The uncertainties in the critical current is estimated at $\pm 1.5\%$; the uncertainties of the transverse pressure are ± 32 MPa and ± 23 MPa for cable samples SMC-RRP-I and -PIT-I, respectively.

sample SMC-PIT-I. In addition, the irreversible reduction sets in quite early, exceeding a level of 2% current degradation at 170 ± 25 MPa for SMC-RRP-I, and 125 ± 10 MPa for SMC-PIT-I. The ‘zero’-pressure initial quench current of SMC-RRP-I is 20.7 ± 1.2 kA at 11.6 ± 0.5 T. The ‘zero’-pressure initial critical current of SMC-PIT-I is 18.0 ± 1.1 kA at 11.4 ± 0.5 T. Both values are similar to the critical currents of the second set of cable samples presented in figure 14. A closer ‘post-mortem’ inspection of the samples revealed a problem with the alignment between the pushing anvil and the cable surface. Although visual inspection revealed only a small angle of about 0.2° between both, subsequent modelling, as reported elsewhere [51], nonetheless indicated that this can have a significant effect on the stress distribution in the cable. It was therefore decided to prepare a second set of cable samples SMC-RRP-II and SMC-PIT-II from the same ‘green’ cable material and to adopt an extra step in the impregnation procedure to improve parallelism, as presented in figure 14.

4.2.3. Decrease of B_{c2} due to transverse pressure. Additional $I_c(B)$ measurements were carried out on SMC-RRP-II and SMC-PIT-II cable samples to gauge the reversible effect of pressure on their upper critical field B_{c2} . These are reported

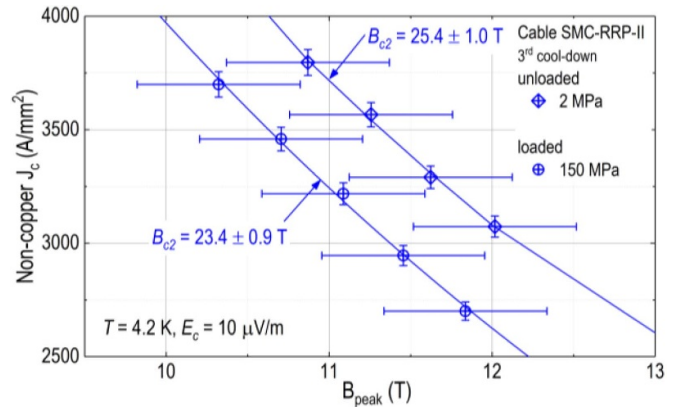


Figure 16. Non-copper critical current density $J_c(B_{peak})$ versus magnetic peak field of the SMC-RRP-II cable sample with ‘zero’ applied stress (about 1 MPa, ‘unloaded’) and exposed to a transverse pressure of 150 MPa (‘loaded’). The unloaded data are measured twice in subsequent cool-down cycles. Solid lines represent the Kramer like fit following equation (5). The uncertainty in critical current is $\pm 1.5\%$, while the peak magnetic field error is ± 0.5 T.

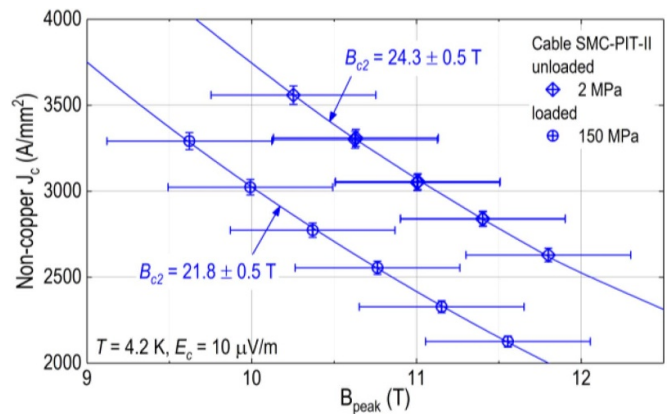


Figure 17. Non-copper critical current density $J_c(B_{peak})$ versus magnetic peak field of the SMC-PIT-II cable sample with ‘zero’ applied stress (about 1 MPa, ‘unloaded’) and exposed to a transverse pressure of 150 MPa (‘loaded’). Solid lines represent the Kramer like fit following equation (5). The error in critical current is $\pm 1.5\%$ while the error in peak magnetic field is ± 0.5 T.

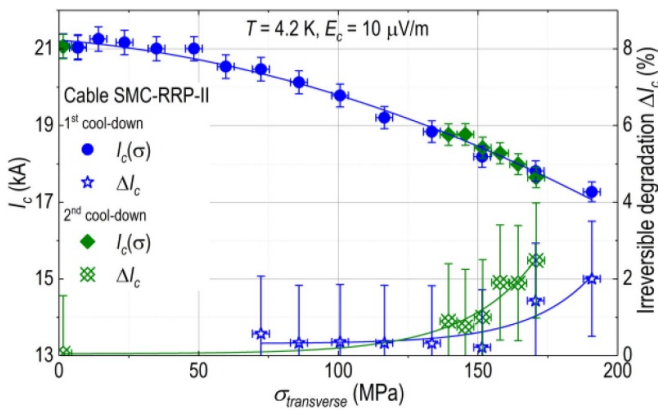
in figures 16 and 17. The no-load $J_c(B_{peak})$ data are discussed in sections 4.1.1 and 4.1.2, where they are compared to witness wire data and to similar measurements carried out at CERN in the test facility (called FRESCA—Facility for the REception of Superconducting Cables) [52]. The data were obtained with the cables subjected to a transverse pressure 150 MPa.

The data sets were characterized in terms of upper critical field and non-copper critical current density at 12 T by fitting them to the Kramer like equation (5). The results are reported in table 11.

Given the 1.5% random error in the critical current measurements, the B_{c2} extrapolation shows ± 1.0 T error. Taking into account this, some significant reduction in B_{c2} and 15% reduction in J_c at 12 T were observed in the SMC-RRP-II sample by application of a transverse pressure of 150 MPa. For

Table 11. Upper critical field and critical current density of SMC cables at 4.2 K, 12 T and different transverse pressure levels.

Cables	σ (MPa)	B_{c2} (T)	J_c (A mm ⁻²)
SMC-RRP-II (1st cool-down)	2	26.4 ± 1.2	3120 ± 190
SMC-RRP-II (3rd cool-down)	2	25.4 ± 1.0	3080 ± 180
SMC-PIT-II	150 ± 3	23.5 ± 0.8	2630 ± 160
	2	24.2 ± 0.5	2520 ± 150
	150 ± 3	21.8 ± 0.3	1900 ± 110

**Figure 18.** Second measurement of the $I_c(\sigma)$ behavior of the sample SMC-RRP-II, in order to check for the influence of a thermal cycle and to narrow down the onset of irreversible degradation more accurately. The solid lines are polynomial fits to the data. Solid symbols represent the normalized critical current $I_c(\sigma)/I_c(0)$ as a function of the transverse stress σ (left axis), open symbols the irreversible degradation ΔI_c (right axis). The solid lines are polynomial fits to the data. The error in critical current is $\pm 1.5\%$; the error in transverse pressure is ± 3 MPa for cable samples SMC-RRR-II and SMC-PIT-II.

sample SMC-PIT-II, the values for the same pressure level are 6% and 25%, respectively.

4.2.4. Single thermal-cycle and load-cycling effects. Cable sample SMC-RRP-II was cooled down a second time and the measurement of critical current versus pressure was repeated in order to check for an influence of thermal relaxation on the pressure-tolerance, as shown also in section 4.1.2, and to measure the onset of irreversible degradation more accurately. The result is shown figure 18. No significant increase in I_c was found and also the pressure dependence of the critical current remained virtually the same.

Also, a series of measurements was performed by which the pressure was cycled between 2 MPa and 150 MPa, in order to check for evolution in the irreversible degradation of the cable samples under cyclic loading and unloading, e.g. due to crack growth in the Nb₃Sn filaments. The results are reported in tables 12 and 13. No significant evolution was observed.

4.2.5. Microscopic analysis of impregnated Nb₃Sn Rutherford cables. After the transverse pressure effect measurements, the samples were carefully removed from the U-shaped holder, cut transversely at the pressed section, embedded in casting

epoxy resin and polished. The cross-sections were examined under an optical microscope to verify the impregnation quality and to investigate for damage of the filaments.

The cross-sectional views of the pressed section of cable sample DS-RRP are shown in figure 19, and significant wire deformation was observed at the edge of the cable. From the close-ups of strands a, b and c, some filamentary damage is visible as well. This is caused by the compaction step in the cabling process.

In figure 20 the cross-sectional views of the pressed section of cable sample DS-PIT-I are shown. The images show that the cable was successfully impregnated as no visible voids are observed. It is found that the stainless-steel core is packed much closer to the left side of the cable with an abnormal ‘wrinkled-up’ shape. The thin-edge of the cable is deformed most, where also most filament damage occurs. The close-ups of strands a, b and c are presented in figures 20(a)–(c). Although significant deformations are observed in the three strands, as well as in some filaments, no visible damage is found.

In the case of cable sample DS-PIT-II, a similar conclusion can be drawn. The cable sample was successfully impregnated and no visible voids and filament damage are observed, as shown in figure 21.

In figure 22 the cross-section of the pressed sections of cable samples SMC-RRP-II and SMC-PIT-II are shown. A stack of dummy and measured cable samples were vacuum impregnated with CTD-101K. Both SMC cable samples were successfully impregnated, and no visible voids were observed. In figures 23 and 24 the close-ups of cross-sectional views of a, b, c strands in cable samples SMC-RRP-II and SMC-PIT-II are shown, and the corresponding position of the strands are indicated in figure 22. Once more, it is concluded that no significant filament damage can be found.

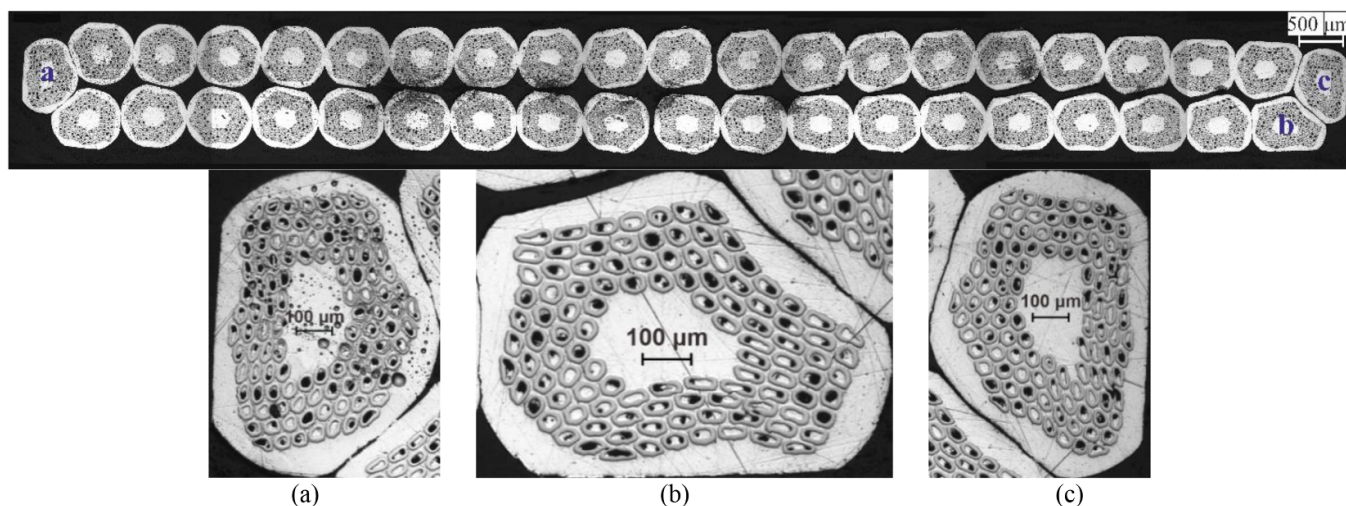
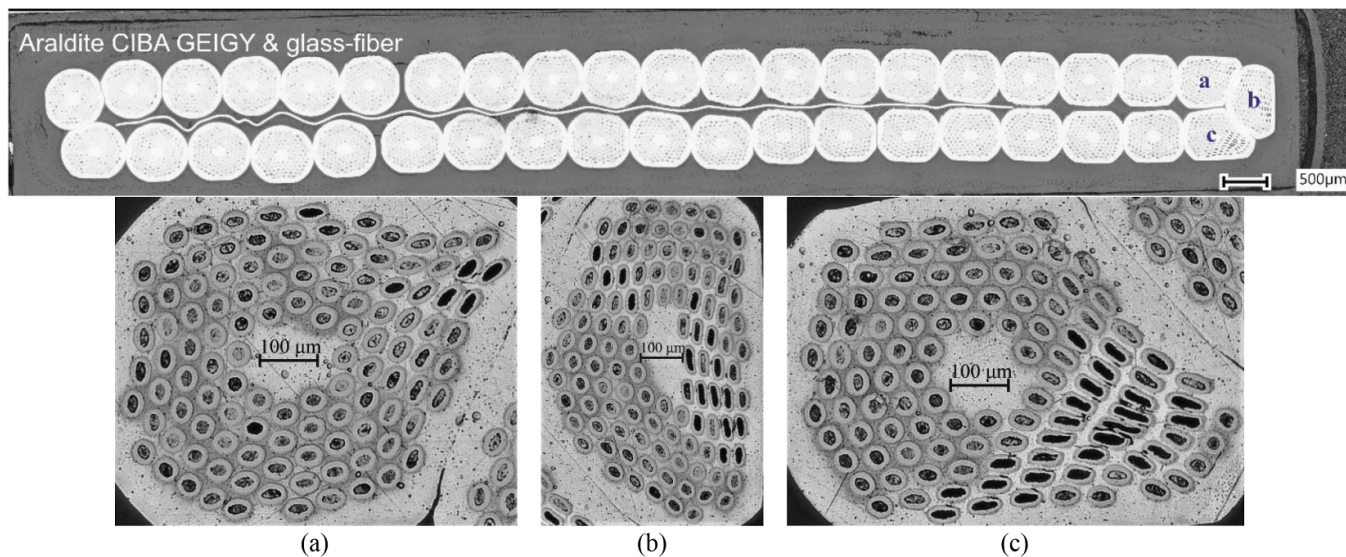
5. Conclusion

The transverse stress susceptibility of various modern Nb₃Sn Rutherford type of cables for use in high-field accelerators magnets were investigated. For this purpose, three key-stoned Nb₃Sn cable samples, called DS-RRP comprising 40 RRP-108/127 type of strands, DS-PIT-I with a stainless-steel core, and DS-PIT-II without core comprising 40 PIT-114 type of strands, were vacuum impregnated with epoxy resin CIBA GEIGY Araldite. In addition, four rectangular Nb₃Sn cable samples called SMC-RRP-I, SMC-RRP-II comprising 18 RRP-132/169 strands; and SMC-PIT-I, SMC-PIT-II cables comprising PIT-192 strands, were vacuum impregnated with epoxy resin CTD-101 K. Moreover, a second set of cable samples SMC-RRP-II and SMC-PIT-II were given an additional ‘alignment’ impregnation, necessary in order to arrive at reliable measurement data of the transverse pressure effect on the critical current.

All cables were successfully impregnated, without leaving bubbles or significant residual voids. The thermal contraction of CIBA GEIGY Araldite and CTD-101K epoxy resins with glass fiber is about 0.2% from room temperature to 4.2 K,

Table 12. Evolution of the critical current of the SMC-RRP-II cable under cyclic loading and unloading. The initial no-load I_c of SMC-RRP-II is 21.1 ± 1.3 kA.

Cycle	SMC-RRP-II (1st cool-down)		SMC-RRP-II (3rd cool-down)	
	I_c (150 MPa) (kA)	I_c (2 MPa) (kA)	I_c (175 MPa) (kA)	I_c (2 MPa) (kA)
1	18.7 ± 1.1	20.9 ± 1.3	18.1 ± 1.1	21.1 ± 1.3
2	18.9 ± 1.1	20.9 ± 1.3	18.1 ± 1.1	21.1 ± 1.3
3	18.7 ± 1.1	20.9 ± 1.3	18.1 ± 1.1	21.1 ± 1.3
4	18.7 ± 1.1	20.9 ± 1.3	18.1 ± 1.1	21.1 ± 1.3

**Figure 19.** Cross-sectional views of the pressed section of cable sample DS-RRP. The cable layout is presented on the top, while close-ups of strands a, b and c at the edge of the cable are shown in bottom pictures.**Figure 20.** Cross-sectional views of the pressed section of cable sample DS-PIT-I. The cable layout is presented on the top, while close-ups of strands a, b and c at the thin-edge of the cable are shown in the bottom pictures.

which is similar to the 0.3% of the reacted Nb_3Sn Rutherford cable samples. Both epoxy resins can be used to successfully enhance the transverse pressure tolerance of Rutherford cables. However, in view of actual coils insulation requirements and the longer pot-life of CTD-101K of 60 h at 40 °C in comparison to the CIBA GEIGY Araldite featuring just 6 h

at 55 °C, the CTD-101K with glass-fiber sleeve presently is more suitable for impregnation of large-size magnets.

The critical current of the cable samples was measured at 4.2 K in a perpendicular applied magnetic field of 10 T. For comparison, the critical current of a virgin witness wire of each cable was measured as a function of the magnetic field

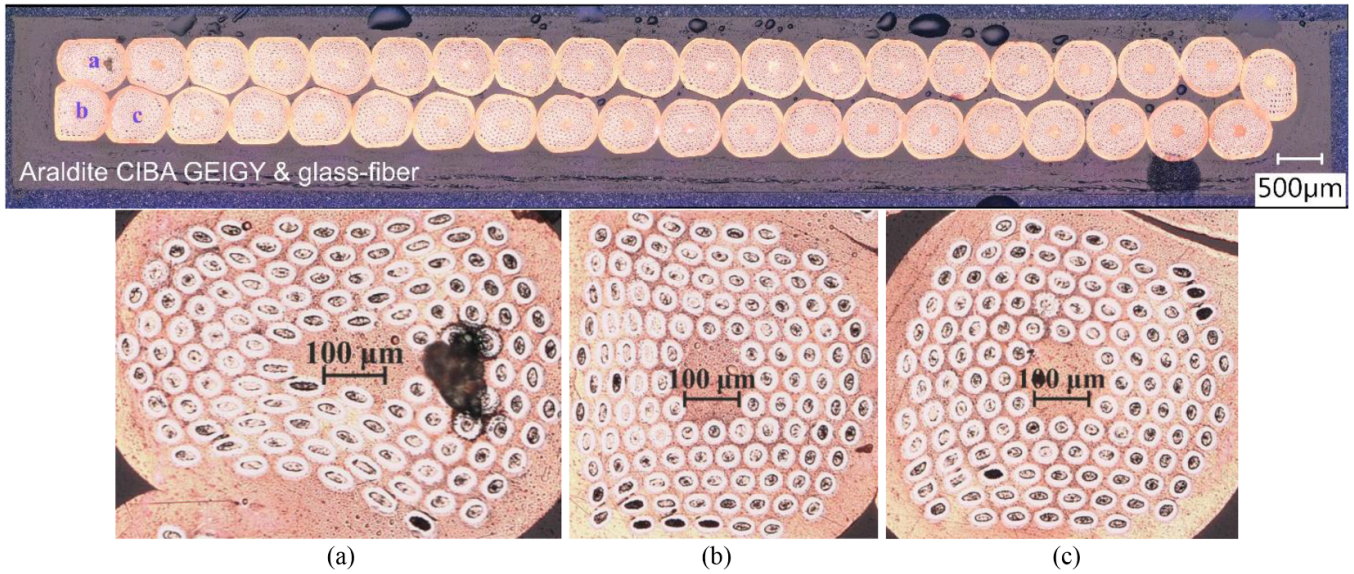


Figure 21. Cross-sectional views of the pressed section of cable sample DS-PIT-II. The cable layout is presented on the top, while close-ups of strands a, b and c at the thin-edge of the cable are shown in the bottom pictures.

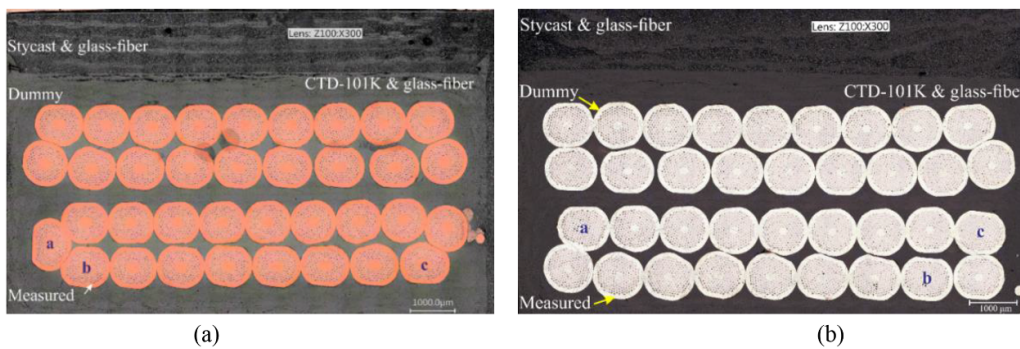


Figure 22. View of the pressed section of cable samples SMC-RRP-II and -PIT-II: (a) SMC-RRP-II; (b) SMC-PIT-II.

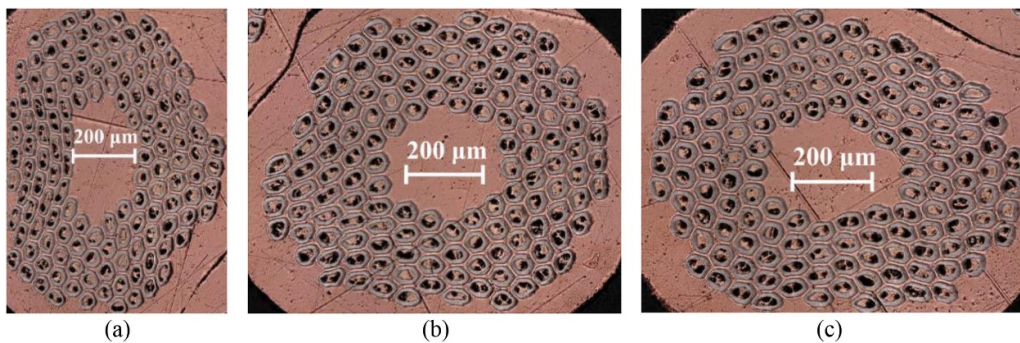


Figure 23. Close-ups of cross-sectional views of strands a, b and c at the thin-edge of cable sample SMC-RRP-II.

as well. Compared to the witness wires, a larger than 25% J_c reduction at 11 ± 0.3 T was observed in cable sample DS-RRP and a 20% J_c reduction was observed in DS-PIT-I. No significant critical current degradation of the remaining DS-PIT cable sample was observed. A possible reason may be the abnormal distribution of the stainless-steel core causing unwanted stress concentration during cabling. The 0.7 mm

diameter RRP-108/127 and PIT-114 wires show a non-copper J_c of 2810 ± 85 A mm⁻² and 2620 ± 80 A mm⁻² at 4.2 K and 12 T, respectively. The 1 mm diameter RRP-132/169 wire has a relatively high non-copper J_c of 3160 ± 190 A mm⁻², while the same size PIT-192 wire has a non-copper J_c of 2480 ± 150 A mm⁻². The RRR values of the SMC virgin wires and extracted strands from the cable samples are larger

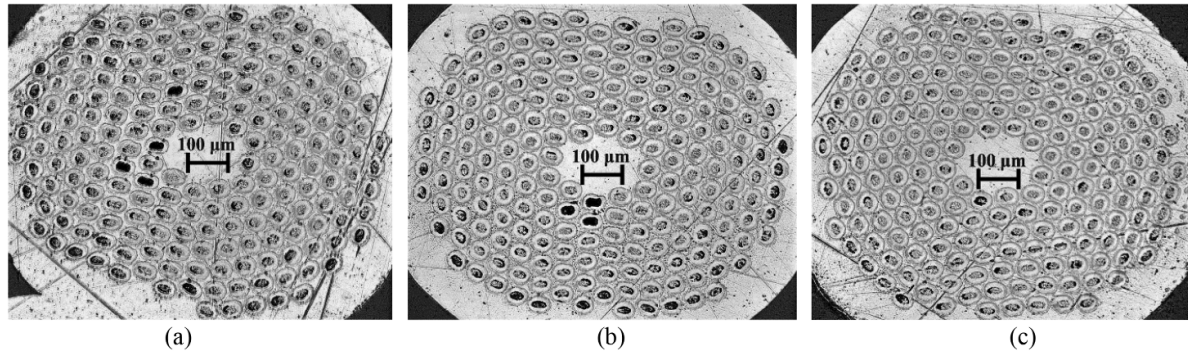


Figure 24. Close-ups of cross-sectional views of strands a, b and c at the thin-edge of cable sample SMC-PIT-II.

Table 13. Evolution of the critical current of the SMC-PIT-II cable under cyclic loading and unloading. The initial no-load I_c of SMC-PIT-II is 18.2 ± 1.1 kA.

Cycle	SMC-PIT-II (1st cool-down)	
	I_c (150 MPa) (kA)	I_c (2 MPa) (kA)
1	14.8 ± 0.9	17.6 ± 1.1
2	14.7 ± 0.9	17.6 ± 1.1
3	14.7 ± 0.9	17.5 ± 1.1
4	14.7 ± 0.9	17.5 ± 1.1
5	14.7 ± 0.9	17.5 ± 1.1

than 100. These values are satisfying the minimum conductor critical current density and RRR requirements of 11 T and 16 T accelerator magnet designs presently under development.

Concerning the transverse stress susceptibility of the cable samples, the critical current decreases reversibly to 90% of the initial 'no-load' values at 250 ± 12 MPa for cable sample DS-RRP; 100 ± 10 MPa for cable sample DS-PIT-I; 70 ± 30 MPa for cable sample DS-PIT-II; 130 ± 3 MPa for cable sample SMC-RRP; and 90 ± 3 MPa for cable sample SMC-PIT. This reversible critical current reduction has to be taken into account when designing magnets as it limits the margin in critical current and stability. No irreversible critical current reduction was observed for cable sample DS-RRP under a transverse pressure up to 250 MPa following the criterion of 2% reduction of critical current at 'zero'-stress. The onset of irreversible critical current degradation is determined at 90 ± 10 MPa for cable sample DS-PIT-I; and 70 ± 30 MPa for cable sample DS-PIT-II. No irreversible critical current reductions were observed for cable samples SMC-RRP and -PIT for a transverse pressure up to 190 MPa and 150 MPa, respectively. The minimum transverse pressure that Rutherford cable need to sustain is estimated at 110 MPa to 150 MPa for 11 T and 150 MPa to 200 MPa for 16 T dipole magnets. Therefore, it is possible to construct dipole magnets using the RRP-108/127 (DS-RRP), RRP-132/169 (SMC-RRP) and PIT-192 (SMC-PIT) wires provided sufficient margin is taken into account. However, to minimize the initial current degradation of the DS-RRP cables, one option is to improve the structure of the wires themselves and make them more robust; the second

option may be using rectangular cable with lower cabling compaction instead of a key-stoned cable. It recommended to perform more measurements on similar cables to confirm the results.

The RRP-132/169 wire is more robust than the present PIT-192 wire. No significant reduction in upper critical field is observed at 150 MPa in cable sample SMC-RRP, but a 6% reduction occurred in cable sample SMC-PIT at the same stress level. Since at this pressure no irreversible critical current was observed in cable samples SMC-RRP-II and SMC-PIT-II, this probably means there is no significant filament cracking in the strands of the Rutherford cable due to the transverse pressure. This is also reflected in the effect of load-cycling on the critical current as no significant critical current reduction was further observed.

The transverse pressure is applied to the cable surface over a length of 45 mm for the DS cables and 46 mm to the SMC cables, whereas the transposition length is 100 mm for DS cables comprising 40 strands and 63 mm for SMC cables comprising 18 strands. Normally, the edge of a rectangular Rutherford cable has lower properties than the center. Especially in a key-stoned Rutherford cable, the thin-edge is the weakest part in the cable and are placed in the maximum magnetic field area. Therefore, incomplete strands in the cable samples are pressed in the measurements, which might result in some level of current redistribution and make the concluded transverse pressure tolerance higher than for the case that all strands are pressed. The effects are not included in data analysis in this paper and are to be studied next.

The comparison of the first and second sets of SMC cable samples, supported by the 2D modelling results reported in [52], shows that special care is needed to avoid stress concentrations. An interface misalignment angle as small as 0.2° can already cause a significant change in the transverse pressure. This demonstrates that measurements of the transverse stress effect on the critical current are delicate and a nearly perfect alignment of pressure block and cable surface must be guaranteed. On the other hand, it should be noted that in real magnets the pressure interfaces will not be ideal as well, and thus large effects and significant spread in magnet performance are to be expected.

Acknowledgments

This work is in the frame of the High-Luminosity LHC and the EuroCirCol projects. The High-Luminosity LHC project was partly financed by the European Commission's seventh framework program (FP7); and the EuroCirCol project was funded by European Union's H2020 framework program under Grant Agreement No. 654305.

ORCID iD

P Gao  <https://orcid.org/0000-0003-4512-056X>

References

- [1] Savary F *et al* 2016 The 11 T dipole for HL-LHC: status and plan *IEEE Trans. Appl. Supercond.* **26** 4005305
- [2] Bajko M *et al* 2011 The Short Model Coil (SMC) dipole: an R&D program towards Nb₃Sn accelerator magnets *IEEE Trans. Appl. Supercond.* **22** 4002704
- [3] Tommasini D *et al* 2018 Status of the 16 T dipole development program for a future hadron collider *IEEE Trans. Appl. Supercond.* **28** 4001305
- [4] Parrell J A, Zhang Y Z, Field M B, Cisek P and Hong S 2003 High field Nb₃Sn conductor development at Oxford Superconducting Technology *IEEE Trans. Appl. Supercond.* **13** 3470–3
- [5] Boutboul T, Oberli L, Ouden A, Pedrini D, Seeber B and Volpini G 2009 Heat treatment optimization studies on PIT Nb₃Sn strand for the NED project *IEEE Trans. Appl. Supercond.* **19** 2564–7
- [6] Barzi E, Turrioni D and Zlobin A V 2014 Progress in Nb₃Sn RRP strand studies and Rutherford cable development at FNAL *IEEE Trans. Appl. Supercond.* **24** 6000808
- [7] Brown M, Tarantini C, Starch W, Oates W, Lee P J and Larbalestier D C 2016 Correlation of filaments distortion and RRR degradation in drawn and rolled PIT and RRP Nb₃Sn wires *Supercond. Sci. Technol.* **29** 084008
- [8] Marinozzi V, Bellomo G, Caiffi B, Fabbriatore P, Farinon S, Ricci A M, Sorbi M and Statera M 2018 Conceptual design of a 16 T cos θ bending dipole for the Future Hadron Collider *IEEE Trans. Appl. Supercond.* **28** 4004205
- [9] Lorin C, Segreti M and Durante M 2018 Design of a Nb₃Sn 16 T block dipole for the Future Circular Collider *IEEE Trans. Appl. Supercond.* **28** 4005005
- [10] Toral F, Munilla J and Salmi T 2018 Magnetic and mechanical design of a 16 T common coil dipole for an FCC *IEEE Trans. Appl. Supercond.* **28** 4004305
- [11] Caspi S, Arbelaez D, Brouwer L, Gourlay S, Prestemon S and Auchmann B 2017 Design of a canted-cosine-theta superconducting dipole magnet for future colliders *IEEE Trans. Appl. Supercond.* **27** 4001505
- [12] Howlett B 1973 Method of fabricating a composite superconductor. Patent US 3728165
- [13] Jakob B and Pasztor G 1989 Effect of transverse compressive stress on the critical current of cabled Nb₃Sn conductor *IEEE Trans. Magn.* **25** 2379–81
- [14] Jakob B, Pasztor G, Bona M and Asner A 1991 Reduced sensitivity of Nb₃Sn epoxy-impregnated cable to transverse stress *Cryogenics* **31** 390–1
- [15] Willering G P, Verweij A P, Scheuerlein C, den Ouden A and Ten Kate H H J 2008 Difference in stability between edge and center in a Rutherford cable *IEEE Trans. Appl. Supercond.* **18** 1253–6
- [16] Pasztor G, Anghel A, Jakob B and Wesche R 1994 Transverse stress effects in Nb₃Sn cables *IEEE Trans. Magn.* **30** 1938–41
- [17] Hashimoto Y, Yoshizaki K and Tanaka M 1974 Processing and properties of superconducting Nb₃Sn filamentary wires *Proc. of the 5th Int. Cryogenic Engineering Conf. (Kyoto, Japan: United Kingdom)* p 332–5 (<https://inis.iaea.org/search/searchsinglerecord.aspx?recordsFor=SingleRecord&RN=7239773>)
- [18] McDonald W K, Curtis C W, Scanlan R M, Larbalestier D C, Marken K and Smathers D B 1983 Manufacture and evaluation of Nb₃Sn conductors fabricated by the MJR method *IEEE Trans. Magn.* **19** 1124–7
- [19] Boschman H, Verweij A P, Wessel S, Ten Kate H H J and van de Klundert L J M 1991 The effect of transverse loads up to 300 MPa on the critical currents of Nb₃Sn cables *IEEE Trans. Magn.* **27** 1831–4
- [20] van Oort J M 2000 Critical current degradation in Nb₃Sn superconductors in accelerator magnets *PhD dissertation* University of Twente, The Netherlands
- [21] Duvauchelle J E, Bordini B, Fleiter J and Ballarino A 2018 Critical current measurements under transverse pressure of a Nb₃Sn Rutherford cable based on 1 mm RRP wires *IEEE Trans. Appl. Supercond.* **28** 4802305
- [22] Bordini B, Alknes P, Ballarino A, Bottura L and Oberli L 2014 Critical current measurements of high- J_c Nb₃Sn Rutherford cables under transverse compression *IEEE Trans. Appl. Supercond.* **24** 9501005
- [23] Ten Kate H H J, Weijers H and van Oort J M 1993 Critical current degradation in Nb₃Sn cables under transverse pressure *IEEE Trans. Appl. Supercond.* **3** 1334–7
- [24] Dietrich D R, Scanlan R M, Walsh R P and Miller J R 1999 Critical current of superconducting Rutherford cable in high magnetic fields with transverse pressure *IEEE Trans. Appl. Supercond.* **9** 122–5
- [25] den Ouden A, Wessel S, Ten Kate H, Kirby G, Taylor T and Siegel N 2000 Conductor development for a wire bore 10 T Nb₃Sn model dipole magnet *IEEE Trans. Appl. Supercond.* **10** 302–5
- [26] Barzi E, Wokas T and Zlobin A V 2005 Sensitivity of Nb₃Sn Rutherford-type cables to transverse pressure *IEEE Trans. Appl. Supercond.* **15** 1541–4
- [27] Zlobin A V *et al* 2005 R&D of Nb₃Sn accelerator magnets at Fermilab *IEEE Trans. Appl. Supercond.* **15** 1113–8
- [28] Godeke A 2005 Performance boundaries in Nb₃Sn superconductors *PhD dissertation* University of Twente, The Netherlands
- [29] 2000 Araldite MY740/HY918/DY062 Vantico Ltd. (<http://www.chemcenters.com/images/suppliers/169257/Araldite%20MY%20740,%20HY%20918,%20DY%20062.pdf>)
- [30] 2007 Araldite MY740/HY906/DY070 Huntsman Advanced Materials
- [31] Hudson P A and Jones H 1981 High field facilities and services of the clarendon laboratory *IEEE Trans. Magn.* **17** 2242–5
- [32] van der Laan M T G, Tax R B and Ten Kate H H J 1992 A 1 T, 0.33 m bore superconducting magnet operating with cryocoolers at 12 K *IEEE Trans. Magn.* **28** 633–6
- [33] den Ouden A, Wessel S, Krooshoop E, Dubbeldam R and Ten Kate H H J 1994 An experimental 11.5 T Nb₃Sn LHC type of dipole magnet *IEEE Trans. Magn.* **30** 2320–3
- [34] Wessel W A J, den Ouden A, Krooshoop H J G, Ten Kate H H J, Wieland J and van der Slot P J M 1999 A conduction-cooled, 680-mm-long warm bore, 3 T Nb₃Sn

- solenoid for a cerenkov free electron laser *IEEE Trans. Appl. Supercond.* **9** 386–9
- [35] CTD-101K 2014 Cryogenic, low viscosity and long pot life, excellent for impregnation of large coils *Composite Technology Development (Lafayette, CO, USA)*
- [36] Kirby G *et al* 2016 Thermal contraction, experimental data and fits for the thermal contraction of future magnet materials at cryogenic temperatures *Internal document of CERN*
- [37] Otten S, Dhallé M, Gao P, Wessel W, Kario A, Kling A and Goldacker W 2015 Enhancement of the transverse tolerance of ReBCO Roebel cables by epoxy impregnation *Supercond. Sci. Technol.* **28** 065014
- [38] Gao P, Wessel W A J, Dhallé M, Otten S, Kario A, van Nugteren J, Kirby G, Bottura L and Ten Kate H 2019 Effect of resin impregnation on the transverse-pressure dependence of the critical current in ReBCO Roebel cables *Supercond. Sci. Technol.* **32** 055006
- [39] van de Camp W 2012 Critical current versus transverse stress and thermal stability of a RRP Nb₃Sn Rutherford cable *Master Thesis* University of Twente, The Netherlands pp 25–27
- [40] 2011 Measurements and error analysis University of North Carolina (<https://www.webassign.net/questionassets/unccolphysmechl1/measurements/manual.html>)
- [41] Gao P 2019 Transverse pressure effect on superconducting Nb₃Sn Rutherford and ReBCO Roebel cables for accelerator magnets *PhD dissertation* University of Twente (<https://doi.org/10.3990/1.9789402816587>)
- [42] Nijhuis A *et al* 2013 The effect of axial and transverse loading on the transport properties of ITER Nb₃Sn strands *Supercond. Sci. Technol.* **26** 084004
- [43] Verweij A P 1990 De invloed van transversale druk op de spanning-stroom karakteristiek van Nb₃Sn-kabels tot 340 MPa en tot 11 T *Master Thesis* University of Twente, The Netherlands
- [44] Bordini B 2010 Self-field correction in critical current measurement of superconducting wires tested on ITER VAMAS barrels *CERN-ITER Collaboration Report* EDMS nr: 1105765
- [45] Bordini B, Ballarino A, Fleiter J, Macchini M and Richter D 2016 11 T conductor performance Review of the 11 T dipoles for the HL-LHC, CERN (<https://indico.cern.ch/event/493351/contributions/1171933/>)
- [46] Bordini B, Duvauchelle J E, Dhalle M, Gao P, Senatore C, Gamperle L and Barth C 2017 Conductor studies 2nd review of the EuroCirCol WP5, CERN (<https://indico.cern.ch/event/661257/contributions/2739628/>)
- [47] Godeke A, Jewell M C, Fischer C M, Squitieri A A, Lee P J and Larbalestier D C 2005 The upper critical field of filamentary Nb₃Sn conductors *J. Appl. Phys.* **97** 093909
- [48] Godeke A, Ten Haken B, Ten Kate H H J and Larbalestier D C 2006 A general scaling relation for the critical current density in Nb₃Sn *Supercond. Sci. Technol.* **19** R100–R116
- [49] Bordini B, Bottura L, Oberli L, Rossi L and Takala E 2012 Impact of the residual resistivity ratio on the Nb₃Sn stability of magnets *IEEE Trans. Appl. Supercond.* **22** 4705804
- [50] Ballarino A and Bottura L 2015 Targets for R&D on Nb₃Sn conductor for High Energy Physics *IEEE Trans. Appl. Supercond.* **25** 6000906
- [51] Gao P, Dhallé M and Ten Kate H 2020 Pressure-induced critical current reduction in impregnated Nb₃Sn Rutherford cables for use in future accelerator magnets *IOP Conf. Ser. Mater. Sci. Eng.* **756** 012015
- [52] Verweij A, Genest J, Knezovic A, Leroy D F, Marzolf J-P and Oberli L R 1999 1.9K test facility for the reception of the superconducting cables for the LHC *IEEE Trans. Appl. Supercond.* **9** 153–6